Sintering temperature effect on electrical transport and magnetoresistance of nanophasic $La_{0.7}Sr_{0.3}MnO_3$

2006 J. Phys.: Condens. Matter 18 8837

(http://iopscience.iop.org/0953-8984/18/39/014)

INSTITUTE OF PHYSICS PUBLISHING JOURNAL OF PHYSICS: CONDENSED MATTER

J. Phys.: Condens. Matter **18** (2006) 8837–8846 doi:10.1088/0953-8984/18/39/014

Sintering temperature effect on electrical transport and magnetoresistance of nanophasic $La_{0.7}Sr_{0.3}MnO_3$

Anurag Gaur and G D Varma[1]

Department of Physics, Indian Institute of Technology Roorkee, Roorkee-247667, India

E-mail: gdvarfph@iitr.ernet.in

Received 26 July 2006, in final form 23 August 2006
Published 15 September 2006
Online at stacks.iop.org/JPhysCM/18/8837

Abstract

Nanophasic $La_{0.7}Sr_{0.3}MnO_3$ (LSMO) samples were prepared by the sol–gel method. The samples were sintered at different temperatures ranging from 600 to 1000 °C. It is shown that the transport and magnetoresistive properties of LSMO samples strongly depend on the sintering temperature (T_s). A substantial decrease in the insulator–metal transition temperature (T_{IM}) and an enhancement in resistivity are found on lowering the sintering temperature. Furthermore, a reduction in magnetization and a slight decrease in paramagnetic–ferromagnetic (PM–FM) transition temperatures (T_c) have been observed as the sintering temperature decreases. The magnetoresistance (MR) at $T < T_c$ increases on decreasing the sintering temperature as well as increasing the applied magnetic field. The enhancement in MR on decreasing the sintering temperature is explained by enhanced spin-polarized tunnelling by assuming an increase of the grain boundary contribution as the sintering temperature decreases.

1. Introduction

The colossal magnetoresistance (CMR) manganites of the type $Ln_{1-x}A_xMnO_3$ (where Ln = La, Pr, Nd, etc, and A is a divalent doping cation) with the perovskite structure have drawn considerable interest in recent years [1, 2]. So far, two CMR effects have been found in these manganites: intrinsic CMR and extrinsic CMR. For most CMR manganites of the $Ln_{1-x}A_xMnO_3$ series, the maximum CMR is obtained near the insulator–metal (IM) transition temperature T_{IM}, accompanied by a simultaneous paramagnetic–ferromagnetic (PM–FM) transition at the Curie temperature (T_c). This is so-called intrinsic CMR [3]. The intrinsic CMR effect, caused by the double exchange (DE) mechanism proposed by Zener in 1951, is useful to explain the CMR phenomenon mostly observed near T_c at a relatively high magnetic field (>10 kOe) [4]. However, the extrinsic CMR, which appears at the temperature $T < T_c$, is

[1] Author to whom any correspondence should be addressed.

related to natural and artificial grain boundaries [5, 6] and is the important source of low-field magnetoresistance (LFMR) in polycrystalline samples. This LFMR or grain boundary MR is due to spin-polarized tunnelling [3] or spin-dependent scattering [5] among neighbouring grains and is important for applications. Although the actual mechanism of the LFMR response for polycrystalline manganite samples is still obscure, it is undoubted that the effect of grain boundaries plays a key role in the LFMR. As a consequence, the preparation of perovskite manganite via the sol–gel method has been a continuous interest [7, 8] because by this technique we can modify the grain boundaries in growing the nanosized particles. So, improved MR could be achieved for nanosized perovskite manganite samples prepared through the sol–gel process. The sol–gel process also has other potential advantages over other traditional processing techniques such as better homogeneities, low processing temperature and improved material properties [9]. Although there are several reports [10–15] on the synthesis of nanophasic manganite by sol–gel based methods, none of them seems to have carried out systematic studies on the effect of sintering temperature on the electrical transport and magnetoresistance of the $La_{0.7}Sr_{0.3}MnO_3$ system.

In this work, we examine the influence of sintering temperature on $La_{0.7}Sr_{0.3}MnO_3$ prepared via the sol–gel process. We observed that the transport and magnetoresistance properties of this $La_{0.7}Sr_{0.3}MnO_3$ system strongly depend on sintering temperature (T_s). As the sintering temperature decreases, the IM transition temperature (T_{IM}) reduces and resistivity increases. Moreover, a decrease in magnetization and PM–FM transition temperature (T_c) is observed as the sintering temperature decreases. An enhancement in magnetoresistance is also observed on decreasing the sintering temperature. These observations are logically explained by assuming the increase of the grain boundary contribution as the sintering temperature decreases [16–18].

2. Experimental procedure

Nanophasic samples of $La_{0.7}Sr_{0.3}MnO_3$ (LSMO) were synthesized via the sol–gel method. The required amounts of high purity nitrates of La, Sr and Mn were dissolved in double distilled water to form an aqueous solution. An equal amount of ethylene glycol was added to this solution with continuous stirring. This solution was then heated on a hot plate at a temperature of ∼80–100 °C until a dry thick brown sol was formed. This was further decomposed in an oven at a temperature of 250 °C to obtain dry fluffy material. The polymeric precursor thus obtained was calcined at 350 °C for 12 h. The resulting powder was separated into parts and pressed in the form of pellets and sintered at 600, 700, 800, 900 and 1000 °C for 12 h. The samples sintered at 600, 700, 800, 900 and 1000 °C are referred to as T6, T7, T8, T9, and T10, respectively. The structural characterization was done by using an x-ray diffraction (Bruker AXS D-8 Advance, Cu Kα radiation) technique at room temperature and the surface morphology was investigated by using a scanning electron microscope (SEM Model LEO 435-VP operating at 15 kV). The temperature dependence of the resistivity of samples was measured by a standard four-probe method using Keithley instruments without or with magnetic fields (0–10 kOe). The DC magnetization measurements were made by using a vibrating sample magnetometer (VSM Model 155, Princeton Applied Research).

3. Results and discussion

X-ray diffraction patterns, recorded at room temperature, of the studied samples are shown in figure 1. The results indicate that all the samples T6, T7, T8, T9 and T10, sintered at 600, 700, 800, 900 and 1000 °C, respectively, correspond to pure LSMO phase with no

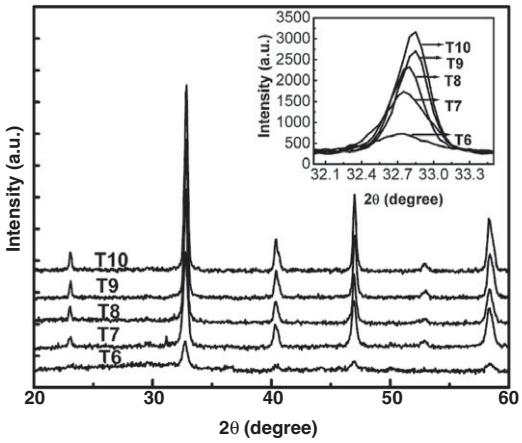

Figure 1. X-ray diffraction patterns of $La_{0.7}Sr_{0.3}MnO_3$ sintered at 600 °C (T6), 700 °C (T7), 800 °C (T8), 900 °C (T9) and 1000 °C (T10). The inset shows the variation in intensity and 2θ of the most intense (121) peak with sintering temperature.

Table 1. Unit cell parameters, cell volume, particle size and grain size of $La_{0.7}Sr_{0.3}MnO_3$ sintered at different temperatures.

Sintering temp.	Unit cell parameters			Unit cell	Particle size	Grain size
T_s (°C)	a (Å)	b (Å)	c (Å)	vol (Å^3)	from XRD (nm)	from SEM (nm)
600	5.486	7.732	5.451	231.2192	31	37
700	5.454	7.709	5.481	230.4480	39	48
800	5.467	7.691	5.465	229.7852	51	66
900	5.426	7.679	5.485	228.5394	56	115
1000	5.417	7.664	5.473	227.2165	60	163

detectable secondary phase within the accuracy of measurement. The pure LSMO phase has been obtained at a sintering temperature as low as 600 °C. The intensity of diffraction peaks for the LSMO perovskite phase increases as the sintering temperature increases from 600 to 1000 °C, indicating that the crystallinity of LSMO becomes better and the particle size increases as the sintering temperature increases. The inset of figure 1 shows the most intense (121) reflection (near $2\theta = 33°$) of T6, T7, T8, T9, and T10 samples. It is clear from the inset that as the sintering temperature increases, the intensity of the (121) reflection increases and there is a decrease in the full width at half maximum (FWHM); hence the particle size increases. The shifting of the (121) peak towards higher values of Bragg angle indicates that the lattice parameter decreases on increasing the sintering temperature. The calculated lattice parameters (orthorhombic unit cell parameters a, b, c) and cell volumes of the unit cell ($V = abc$) are shown in table 1. It is observed that the cell volume of the unit cell decreases as the sintering temperature increases. The average particle sizes of the samples are determined from x-ray data using Scherrer's formula (PS $\sim K\lambda/\beta\cos\theta$, where $k \sim 0.89$ is the shape factor, λ is the wavelength of the x-rays, β is the FWHM and θ is the Bragg angle) [19]. The calculated average particle sizes are ∼31, ∼39, ∼51, ∼56 and ∼60 nm for the samples sintered at 600, 700, 800, 900 and 1000 °C, respectively. The representative SEM images of the samples T7, T8, T9, and T10 are shown in figures 2(a)–(d), respectively. It can be seen from figure 2 that the grain boundaries in sample T7 are not clear and there is a long neck between two grains. With

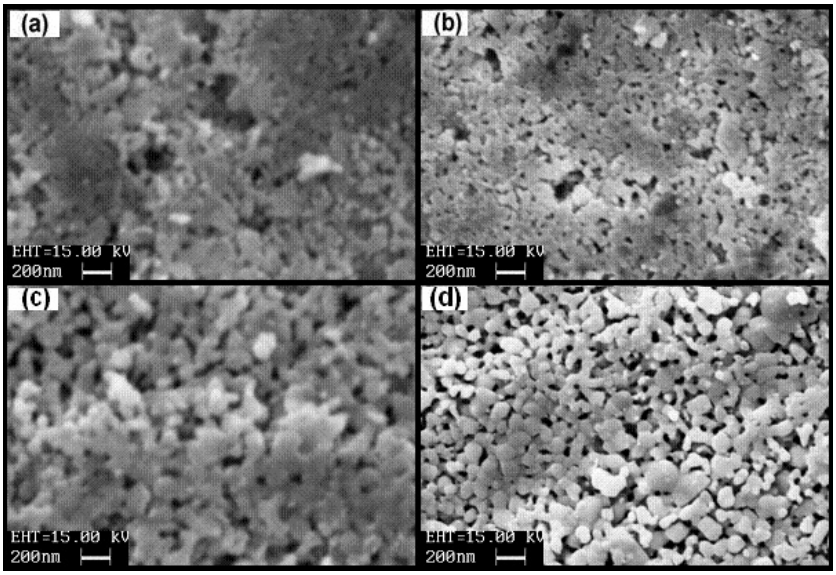

Figure 2. Scanning electron micrographs of $La_{0.7}Sr_{0.3}MnO_3$ sintered at different temperatures: (a) 700 °C (T7), (b) 800 °C (T8), (c) 900 °C (T9) and (d) 1000 °C (T10).

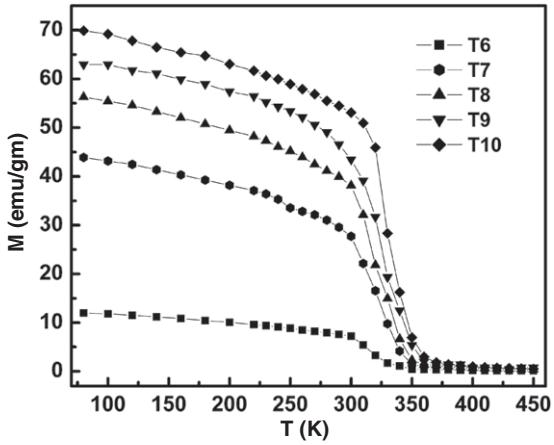

Figure 3. Temperature dependence of magnetization at 5 kOe of $La_{0.7}Sr_{0.3}MnO_3$ sintered at different temperatures.

the increase of sintering temperature from sample T7 to sample T10, the grain size becomes larger, the grain boundaries become obvious, and the necks between grains disappear. When the grain size becomes larger, the grain boundary effects should also decrease from sample T7 to sample T10 because of the decrease in number of grain boundaries. The average grain sizes measured from SEM micrographs are ∼37, ∼48, ∼66, ∼115 and ∼163 nm for the samples T6, T7, T8, T9, and T10, respectively.

The magnetization curves of all the samples measured under 5 kOe field in the temperature range 80–300 K are shown in figure 3. All the samples show the PM–FM transition at a particular temperature (T_c). We observed a slight variation in T_c for the samples sintered at

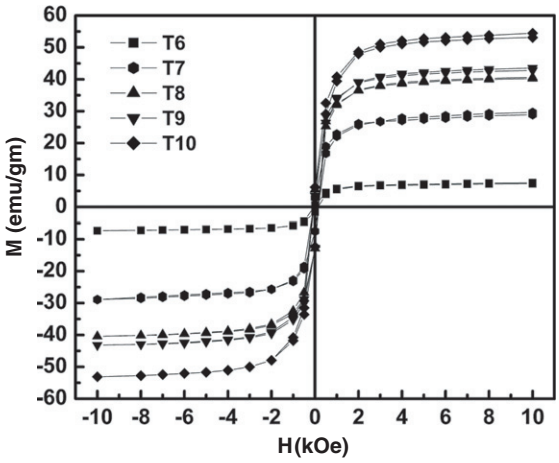

Figure 4. Field dependence of magnetization (M–H) curves at room temperature of $La_{0.7}Sr_{0.3}MnO_3$ sintered at different temperatures.

different temperatures. The transition temperatures determined from the peak in dM/dT–T curves are found to be ∼311, ∼321, ∼324, ∼326 and ∼330 K for the samples T6, T7, T8, T9, and T10, respectively. Moreover, the magnetization also decreases as the sintering temperature decreases. The value of magnetization (M) at 80 K for the samples T6, T7, T8, T9 and T10 are 11.96, 43.88, 56.28, 62.95 and 69.88 emu g^{-1}, respectively. This may be because of the formation of extra grain boundaries as the sintering temperature decreases, leading to enhanced broken bonds at the surface, which cause decreases in the magnetization value. This is the most general observation in the case of nanoparticles of the manganite system [16, 20]. However, a report by Fu [21] on the $La_{0.8}Ca_{0.2}MnO_3$ nanoparticle system shows results contradicting the above facts on reduced particle size. He reported that the magnetization increases as the particle size decreases due to strain at the grain boundaries. Zhang *et al* also analysed in detail the effect of the annealing on the magnetization for various x values in the $La_{1-x}Sr_xMnO_3$ system [22]. They found that at low doping ($x < 0.25$), the magnetization decreases with an increase in sintering temperature, and for higher doping ($x > 0.25$), the magnetization increases with an increase in sintering temperature. So our results support those of Zhang *et al* [22], i.e. for $x > 0.25$ the magnetization decreases on decreasing the sintering temperature, or particle size and grain boundaries play the important role in the reduction of magnetization. The magnetization versus field (M–H) curves at room temperature for the studied samples are displayed in figure 4. The M–H curves also show that the magnetization of the samples decreases on decreasing the sintering temperature. This demonstrates that ferromagnetic order is weakened and magnetic disorder increases on reducing the sintering temperature.

The temperature dependence of resistivity at zero field measured in the temperature range 80–300 K for the studied samples is shown in figure 5. The resistivity of the samples increases as the sintering temperature or particle size decreases. The values of resistivity are 59.19, 1.59, 0.76, 0.39 and 0.14 Ω cm at room temperature (300 K) for the samples T6, T7, T8, T9 and T10, respectively. Thus, the resistivity of sample T6 increases by more than one order of magnitude as compared to sample T10. This increase in resistivity is caused by enhanced scattering of the charge carriers by increasing the number of grain boundaries as the sintering temperature decreases. On increasing the sintering temperature, the particle size increases, leading to a decrease in the number of grain boundaries and magnetic disorder. This causes a decrease in

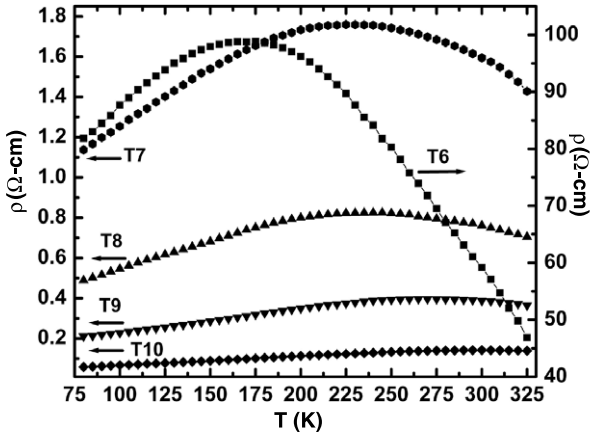

Figure 5. Temperature dependence of the resistivity at zero field of $La_{0.7}Sr_{0.3}MnO_3$ sintered at different temperatures.

scattering of the carriers and hence a decrease in the resistivity. All the studied samples show an insulator ($d\rho/dT < 0$) to metal ($d\rho/dT > 0$) transition on lowering the temperature at a particular value (T_{IM}). The values of the insulator to metal transition temperature are ∼175, ∼228, ∼245, ∼273 and ∼303 K for the samples T6, T7, T8, T9 and T10, respectively. Thus the value of the transition temperature decreases from 303 to 175 K as the sintering temperature decreases from 1000 to 600 °C. T_{IM} is an extrinsic property and strongly depends on the synthesis condition and microstructure (e.g. grain boundaries). The strong suppression in the value of T_{IM} on decreasing the sintering temperature is due to suppression of the DE mechanism because of the increase in non-magnetic phase fraction, which is due to enhanced number of grain boundaries as a consequence of the lower sintering temperature. Thus lowering the sintering temperature reduces the metallic transition temperature and increases the resistivity. It is also noted that there is a large difference between the value of T_{IM} and T_c for the samples sintered at lower temperatures. The variation of T_{IM} and T_c with sintering temperature is shown in figure 6. From the figure it is clear that there is a substantial decrease in T_{IM} (from 303 to 175 K) when the sintering temperature decreases from 1000 to 600 °C, whereas T_c decreases only marginally (from 330 to 311 K). This difference is due to the fact that T_c is an intrinsic property and does not show much dependence on sintering temperature while T_{IM} is an extrinsic property that strongly depends upon the grain boundaries and hence the sintering temperature [23].

The temperature dependence of magnetoresistance (MR) for the studied samples measured in the range 80–300 K at fields of 1 and 10 kOe is shown in figure 7. The MR ratio is defined as MR (%) $= [\rho(0, T) - \rho(H, T)]/\rho(H, T) \times 100\%$, where $\rho(0, T)$ and $\rho(H, T)$ are the resistivity values for zero and applied fields, respectively. The MR of all the samples measured at 1 and 10 kOe increases on lowering the sintering temperature. The MR values at 80 K are 15.3%, 12.9%, 10.8%, 9.4% and 7.9% at 1 kOe and 28.9%, 26.5%, 24.1%, 22.5% and 21.1% at 10 kOe for the samples T6, T7, T8, T9 and T10, respectively (as shown in table 2). The measurements of MR at both fields reveal that the maximum MR is observed for the sample T6, sintered at the lowest temperature (600 °C). This enhancement in MR basically arises due to the intergrain spin-polarized tunnelling across the grain boundaries at $T < T_c$ as proposed by Hwang *et al* [3]. The existence of grain boundaries and the nature of the grain boundary are key ingredients in the mechanism of electric transport, since they constitute the barriers through

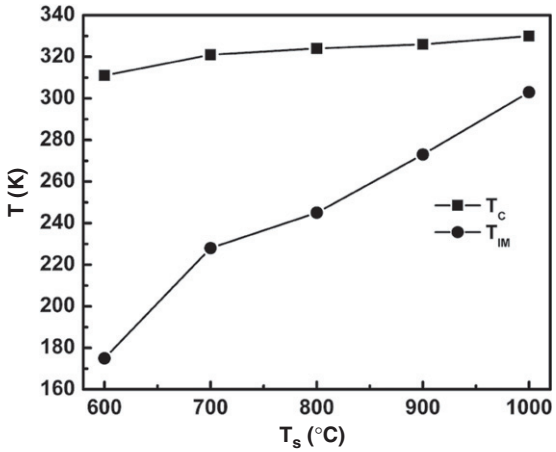

Figure 6. Variation of insulator–metal transition temperature (T_{IM}) and PM–FM transition temperature (T_c) with sintering temperatures.

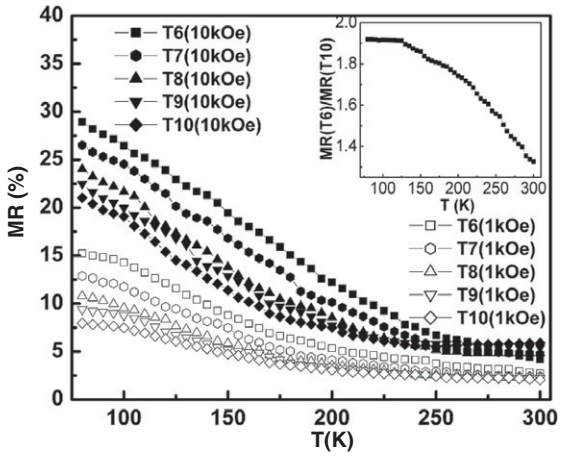

Figure 7. Temperature dependence of the magnetoresistance (MR) in fields of 1 kOe and 10 kOe of $La_{0.7}Sr_{0.3}MnO_3$ sintered at different temperatures. The inset shows the MR (T6)/MR (T10) ratio with temperature at 1 kOe.

which carriers should cross or tunnel [3]. The grain boundary contribution usually increases on decreasing the sintering temperature. So, in our samples the low field magnetoresistance (LFMR) increases on decreasing the sintering temperature because of enhanced spin-polarized tunnelling through the increased number of grain boundaries as the sintering temperature decreases. So, in the present case, the LFMR increases with decreasing sintering temperature because we are increasing the disordered surface by decreasing the sintering temperature or particle size [16, 17]. The reduction in magnetization on decreasing the sintering temperature (figure 3) also supports the magnetic spin disorder induced by grain boundaries in samples sintered at lower temperatures, and this spin disorder is suppressed by applying the magnetic field, resulting in the enhancement in MR. The variation of the ratio of MR of samples T6 and T10, measured at 1 kOe, with temperature is shown in the inset of figure 7. It shows that the ratio of MR increases on decreasing the temperature, and the MR of sample T6 at 80 K is

Table 2. Insulator–metal transition temperature (T_{IM}), paramagnetic–ferromagnetic transition temperature (T_c) and magnetoresistance (MR) of $La_{0.7}Sr_{0.3}MnO_3$ sintered at different temperatures.

			MR (%) at 80 K	
T_s (°C)	T_{IM} (K)	T_c (K)	1 kOe	10 kOe
600	175	311	15.3	28.9
700	228	321	12.9	26.5
800	245	324	10.8	24.1
900	273	326	9.4	22.5
1000	303	330	7.9	21.1

almost two times the MR of sample T10 at 1 kOe, while it is 1.4 times that at 10 kOe. Moreover, as we go from sample T10 to T6, the value of MR at 80 K increases from 7.9% to 15.3% at 1 kOe and 21.1% to 28.9% at 10 kOe (see table 2). This shows that the percentage change in MR from sample T10 to T6 is more at low field (1 kOe) as compared to higher field (10 kOe). Continuous enhancement in MR on decreasing the temperature (from 300 to 80 K) also supports its low field magnetoresistance behaviour. As Hwang *et al* [3] demonstrated, the MR in the polycrystalline samples exhibits two distinct regions: large MR at low fields dominated by spin-polarized tunnelling between grains, and high field MR which is remarkably temperature independent from 5 to 280 K. They also showed that the low field MR caused through spin-polarized tunnelling increases on decreasing the temperature and the high field MR above 0.5 T remains temperature independent over a wide range from 5 to 280 K. In our case, the MR is not constant with temperature and it increases on decreasing the temperature for both (1 and 10 kOe) field scales, which demonstrates that this enhanced MR is the first type, i.e., this is low field MR dominated by spin-polarized tunnelling through an increased number of grain boundaries as the sintering temperature decreases. In present case, this low field MR behaviour is up to 10 kOe, which is possibly due to our low sintering temperature as compared to the 1300 and 1700 °C sintering temperatures of Hwang *et al*. So in our case the spin-polarized tunnelling phenomenon is more effective due to the enhanced number of grain boundaries as the sintering temperature is low. Therefore, the present enhancement in MR up to 10 kOe is low field MR caused by enhanced spin-polarized tunnelling through and increased number of grain boundaries as the sintering temperature decreases.

The magnetic field dependence of MR for all the studied samples measured in magnetic field range 0–12 kOe at 80 K is shown in figure 8. Analysis of figure 8 shows that with increase in the magnetic field from 0 to 12 kOe, the MR of all the samples increases on increasing the magnetic field. Moreover, as the sintering temperature decreases, the MR increases. The maximum MR is observed in sample T6, sintered at the lowest temperature (600 °C). The value of MR at 80 K for the sample T6 is 30.3% while it is 22.1% for the sample T10 at 12 kOe. It should also be noted that the variation of MR does not show any saturation in MR even up to 12 kOe. This enhancement in MR as the sintering temperature decreases is again caused by spin-polarized tunnelling at the grain boundaries.

4. Conclusions

In summary, we studied the electrical and magnetotransport properties of nanophasic $La_{0.7}Sr_{0.3}MnO_3$ samples prepared by the sol–gel process. All the samples have pure LSMO perovskite phase with orthorhombic unit cells. Both T_{IM} and T_c shift towards lower temperature and the magnetization decreases on decreasing the sintering temperature. Moreover, T_{IM}

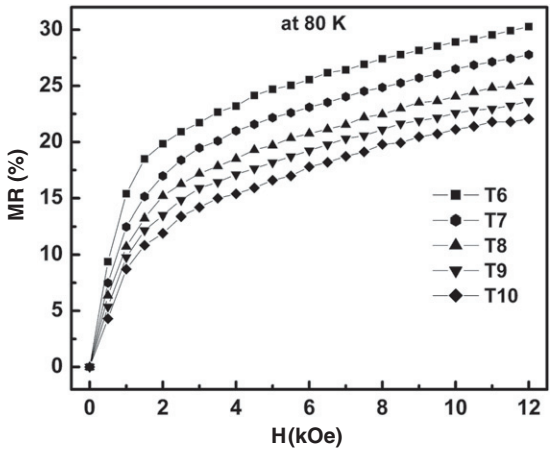

Figure 8. Field dependence of the magnetoresistance (MR) in the range 0–12 kOe at 80 K of $La_{0.7}Sr_{0.3}MnO_3$ sintered at different temperatures.

decreases substantially from 303 to 175 K while T_c shows only a slight decrease from 330 to 311 K. It has been observed that the low field magnetoresistance at $T < T_c$ increases as the sintering temperature decreases. This enhancement in LFMR for the samples sintered at lower temperature is due to enhanced spin-polarized tunnelling by increasing the grain boundary contribution as the sintering temperature decreases.

Acknowledgments

The authors are grateful to Professor O N Srivastava, Professor D Pandey (BHU) and Dr H K Singh (NPL) for helpful discussions and encouragement. One of the authors (AG) is grateful to the University Grant Commission (UGC), New Delhi, for the award of a Senior Research Fellowship.

References

[1] Nagaev E L 2001 *Phys. Rep.* **346** 387
[2] Rao C N R, Mahesh R, Raychaudhuri A K and Mahendiran R 1998 *J. Phys. Chem. Solids* **59** 487
[3] Hwang H Y, Cheong S W, Ong N P and Batlogg B 1996 *Phys. Rev. Lett.* **77** 2041
[4] Zener C 1951 *Phys. Rev.* **82** 403
[5] Gupta A and Sun J Z 1999 *J. Magn. Magn. Mater.* **200** 24
[6] Issac S P, Mathur N D, Evetts J E and Blamire M G 1998 *Appl. Phys. Lett.* **72** 2038
[7] Mahesh R, Mahendiran R, Raychaudhuri A K and Rao C N R 1996 *Appl. Phys. Lett.* **68** 2291
[8] Vazquez-Vazquez C, Blanco M C, Lopez-Quintela M A, Sanchez R D, Rivas J and Oseroff S 1998 *J. Mater. Chem.* **8** 991
[9] Brinker C J and Scheres G W 1990 *Sol–Gel Science* (New York: Academic)
[10] Lisboa-Filho P N, Mombru A W, Pardo H, Ortiz W A and Leite E R 2003 *J. Phys. Chem. Solids* **64** 583
[11] Vertruyen B, Rulmont A, Cloots R, Ausloos M, Dorbolo S and Vanderbemden P 2002 *Mater. Lett.* **57** 598
[12] Mahesh R, Mahendiran R, Raychaudhary A K and Rao C N R 1996 *Appl. Phys. Lett.* **68** 2291
[13] Shankar K S, Kar S, Subbanna G N and Raychaudhuri A K 2004 *Solid State Commun.* **129** 479
[14] Li R W, Xiong H, Sun J R, Li Q A, Wang J H, Zhang J and Shen B G 2001 *J. Phys.: Condens. Matter* **13** 141
[15] Muroi M, Street R and McCormick P G 2000 *J. Appl. Phys.* **87** 5579
[16] Balcells L I, Fontcuberta J, Martinez B and Obradors X 1998 *Phys. Rev.* B **58** R14697
[17] Zhu T, Shen B G, Sun J R, Zhao H W and Zhan W S 2001 *Appl. Phys. Lett.* **78** 3863

[18] Wang Z H, Ji T H, Wang Y Q, Chen X, Li R W, Cai J W, Sun J R, Shen B G and Yan C H 2000 *J. Appl. Phys.* **87** 5582
[19] De Keiyser Th H, Langford J I, Mittemeijer and Vogels A B P 1982 *J. Appl. Crystallogr.* **15** 308
[20] Rivas J, Hueso L E, Fondado A, Rivadullo F and Lopez-Quintela M A 2000 *J. Magn. Magn. Mater.* **221** 57
[21] Fu Y 2000 *Appl. Phys. Lett.* **77** 118
[22] Zhang N, Yang W, Ding W, Xing D and Du Y 1999 *Solid State Commun.* **109** 537
[23] Andres A de, Garcia-Hernandez M and Martinez J L 1999 *Appl. Phys. Lett.* **74** 3884